

# Hydrogen in stationary applications: Coupling the electricity, gas and mobility sectors (Digi-HyPro)

Julián Puszkiet\*, Myriam Covarrubias  
Guraneros, Lukas Fleming, Thomas  
Friedrich Johannes Kaufmann, Phillip  
Krause, Jan Warfsmann, Eike Wienken,  
Lukas Wildner, Matthias Schulze,  
Thomas Klassen, Julian Jepsen

Faculty of Mechanical Engineering, Institute of Material  
Engineering, Helmut-Schmidt-University, Hamburg,  
Germany

\*puszkietj@hsu-hh.de

Julián Puszkiet\*, Myriam Covarrubias  
Guraneros, Lukas Fleming, Thomas  
Friedrich Johannes Kaufmann, Phillip  
Krause, Jan Warfsmann, Eike Wienken,  
Lukas Wildner, Helge Kutzner, Gökhan  
Gizer, José María Bellosta von Colbe,  
Klaus Taube, Thomas Klassen, Julian  
Jepsen

Institute of Hydrogen Technology, Helmholtz-Zentrum

Hereon, Geesthacht, Germany

\*julian.puszkiet@hereon.de

Homa Hamed, Torsten Brinkmann\*

Institute of Membrane Research, Helmholtz-Zentrum

Hereon, Geesthacht, Germany

\*torsten.brinkmann@hereon.de

**Abstract** – Global warming and continuous fossil fuel depletion are worldwide phenomena that pose challenges such as the reduction of greenhouse gas emissions and the further exploitation of renewable energy sources. Nevertheless, the transition from fossil fuels to a renewable-energy-based economy demands more innovative solutions and developments such as the Power-to-Gas-to-Power (PtoGtoP) idea. Hydrogen is considered one of the clean energy carriers in the concept of PtoGtoP. However, this strategy still suffers from several challenges, like intermittent inflows of energy, high costs, and rather low energy efficiency due to the losses during conversion and storage. The goal of the Digi-HyPro (Digitalized Hydrogen Process Chain for the Energy Transition) project is to develop an efficient and modular PtoGtoP system. The concept of this modular system, called Smart-Energy-Transform-Unit (SET-Unit), aims to design a decentralized and scalable system for clean energy demands spreading across different locations. The SET-Unit serves to optimize the connections between renewable sources and the current power and gas grid demand. Applying this concept, hydrogen generated by an electrolyzer can be stored compactly and safely in a metal hydride storage system or fed into the natural gas grid. On-demand, hydrogen can also be taken from the intermediate storage facility or the gas grid by applying gas separation techniques and can be delivered (i) to an integrated fuel cell to produce power or (ii) to a metal hydride compressor to provide hydrogen for the mobility sector (trucks, cars, trains, etc.). Component and system level simulations are performed to design, develop and optimize the individual and overall integrated system. These digital models draw critical data from experiments and are validated using prototype setups. For this purpose, experimental setups on a laboratory scale of 10 kWel, and an intermediate scale of 50 kWel are part of the Digi-HyPro project's plan. This multidisciplinary investigation involves the optimization of the digital SET-Unit system with experimental demonstrations in kWel ranges. Final scalability studies in the industrially relevant MWel range can pave the way to an efficiently networked green energy system.

**Keywords** – Green Hydrogen Production, Sector Coupling, Metal Hydrides, Hydrogen Purification, Gas-Grid-Based Hydrogen Storage

## NOMENCLATURE

AB <sub>2</sub> -alloy	Room temperature hydride forming alloy based on Ti-Zr (A) and Cr-Mn-V-Fe (B)
AB <sub>5</sub> -alloy	Room temperature hydride forming alloy based on La-Ce-Pr-Nd (A) and Ni-Mn-Co-Al (B)
AEM	Anion Exchange Membrane
Digi-HyPro	Digitilized Hydrogen Process Chain for the Energy Transition
EL	Electrolyzer
ENG	Expanded Natural Graphite
FC	Fuel Cell
FEM	Finite Element Modeling
HTF	Heat Transfer Fluid
MH	Metal Hydride
NG	Natural Gas
PEM	Proton Exchange Membrane
PSA	Pressure Swing Adsorption
PtoGtoP	Power-to-Gas-to-Power
RT	Room Temperature
SET-Unit	Smart-Energy-Transform-Unit
SIM	System Integration Modeling
TRL	Technology Readiness Level

## I. INTRODUCTION

The worldwide dependency on non-renewable fossil fuel resources [1], the increase in energy demand [2], and the rise in the earth's average surface temperature owing to global warming [3] request the short-term introduction of renewable energy sources [4]. Hydrogen is considered one of the clean energy carriers required to implement the PtoGtoP concept. However, this strategy still suffers from several challenges, like intermittent inflows of energy, high costs, and low energy efficiency (15 to 40 %) due to the losses during conversion and storage [5]. One of the main bottlenecks to improve the



## II. EXPERIMENTAL AND MODEL DESCRIPTION

In this section, the experimental procedures and modeling descriptions are presented. In the case of the MH material for storage and compression, the synthesis, characterization, and surface modification techniques are described. The software, the physics included, and the relevant parameters introduced in the models are shown for the FEM and SIM.

### A. Characterization and surface modifications of MH forming alloy for hydrogen storage

The commercially available metal alloy HydrallloyC5 (AB2-alloy; Ti<sub>0.95</sub>Zr<sub>0.05</sub>Mn<sub>1.46</sub>V<sub>0.45</sub>Fe<sub>0.09</sub>) was purchased from GfE (Gesellschaft für Elektrometallurgie). The particle size of the Hydrallloy C5 was reduced from 2-10 mm down to  $\leq 4$  mm before use with a Retsch BB50 jaw crusher. ENG (particle size 5  $\mu$ m; SGL-Carbon) and Aerosil R805 (Evonik Operations) have been used as received. For the experiments, the HydrallloyC5 has been used as pure material or in combination with ENG and Aerosil. In a typical experiment, 10 g of Hydrallloy was placed with ENG (1 g; 10 wt%) and optionally Aerosil R805 (0.02 g; 0.2 wt%) in a round-bottom flask and mixed for 2 h with a mechanical stirrer at RT. The characterization of the sample was done with an in-house produced Sieverts apparatus. In addition to the hydrogen capacity, the temperature and strain were also measured in situ by attaching a strain gauge and thermocouple to the sample holder. In a typical experiment, the sample holder was filled with about 8 g of sample, and the conditions were set to 40 °C / 40 bar hydrogen pressure (absorption) and 40 °C / 5 bar hydrogen pressure (desorption). The hydrogen capacity and temperature behavior of the samples were evaluated during 50 hydrogenation-dehydrogenation cycles, while the stress behavior was evaluated for 7 to 16 hydrogenation-dehydrogenation cycles.

### B. Synthesis and Characterization of MH forming alloy for hydrogen compression

TiCr<sub>1.9</sub> alloy was synthesized by using and Edmund Bühler MAM-1 arc melter. The desired mass of Ti and Cr foils were weighed to form the TiCr<sub>1.9</sub> composition. In total, 4 g of material was placed into the melting chamber. Ti and Cr were melted together with an electric arc and cooled to room temperature. The prepared alloy was inverted and remelted five times to obtain a homogeneous product. The synthesized alloy was crushed into small pieces and stored in air. Diffraction patterns of as-synthesized and hydrogenated samples were collected using a Bruker D8 Discover diffractometer, equipped with a 2D Vantec detector. Cu K $\alpha$  radiation was used and the Bragg angle was chosen between 30-80°. Phase analysis of as-synthesized and hydrogenated samples was carried out via MAUD software with the Rietveld approach [10, 11]. Hydrogenation of the samples for the diffraction experiment was carried out using a Sieverts apparatus, Hera (QC J4G 1A1, Canada) [12]. The reactor with the hydrogenated sample was cooled to the liquid nitrogen temperature for ~30 minutes followed by the evacuation of the cooled reactor for ~1 minute. Then, the sample was exposed to air and further kept at liquid nitrogen temperature for 30 minutes. The reactor was at that moment opened to air, and the diffraction pattern of the sample was collected immediately.

Pressure composition isotherms were collected using a Sieverts apparatus PCTPro-2000 (Hy-energy LLC). 2 g of alloy, cut into small pieces, were placed in the sample chamber. For activation, the sample was firstly evacuated at

8 °C, and hydrogenated under 120 bar of H<sub>2</sub> at room temperature. Pressure-Composition isotherms were collected at five different temperatures: 15 °C, 5 °C, 0 °C, - 5 °C and -10 °C. Enthalpy and entropy of the sample were experimentally calculated, and the dependence of equilibrium pressure against temperature was plotted using the van't Hoff equation.

### C. Finite element modeling description

The modeling of the MH-storage and compressor vessels was performed using the FEM software COMSOL 5.6. It includes the modeling of heat, momentum and mass transfer. The most important assumptions for the modeling of such MH-based vessels were: 1. the hydride bed was modeled as isotropic and 2. local thermal equilibrium between the solid particles of the hydride bed and the gas phase. The hydrogen was modeled as an ideal gas and the expansion of the metal hydride due to the absorption of hydrogen was not taken into account. To model the transport of hydrogen, in the case of the MH-storage vessel, Darcy's law was applied, while for the MH-compressor vessels, the Brinkman equation was utilized. In both cases, the thermodynamic behavior of the MH compounds was described by the van't Hoff EQUATION 1:

$$p_{eq} = \exp(\Delta H / (R * T) - \Delta S / R) \quad (1),$$

where,  $p_{eq}$  [bar] represents the equilibrium pressure of the MH-M system,  $\Delta H$  [kJ/mol H<sub>2</sub>] and  $\Delta S$  [J/mol H<sub>2</sub> K] are the enthalpy and entropy changes,  $T$  [K] is the temperature, and  $R$  [J/ mol K] the ideal gas constant.

The kinetic behavior of the hydrides was implemented by applying the differential form of the separable variable EQUATION 2 [13].

$$d\alpha/dt = K(T) * F(p, p_{eq}) * G(\alpha) \quad (2),$$

where,  $\alpha$  represents the hydrogen absorbed/desorbed fraction, i.e., mass of hydrogen absorbed during the process over the maximum reached hydrogen mass,  $K(T)$  is the temperature functionality described by the Arrhenius's dependency,  $F(p, p_{eq})$  is the pressure functionality dependent on the operative pressure and the equilibrium pressure  $p_{eq}$ , and  $G(\alpha)$  is the description of the rate-limiting step of the reaction.

TABLE I shows the metal hydride forming material properties used in the MH-storage and compressor vessel simulations:

TABLE I: MATERIAL PROPERTIES FOR FEM SIMULATIONS OF MH-STORAGE AND COMPRESSOR VESSELS

Properties	Hydrallloy C5	Ref.	AB <sub>2</sub> -Alloy	Ref.
$\rho_{metal}$	6379 [kg/m <sup>3</sup> ]	This work	6240 [kg/m <sup>3</sup> ]	[18]
$wt_{max}$	1.1-1.2 [wt%]	This work	1.4 [wt%]	[18]
$\Delta H_{Abs}$ $\Delta H_{Des}$	- 22.3 [kJ/mol] 28.4 [kJ/mol]	[14]	- 22 [kJ/mol] 24 [kJ/mol]	[18]
$\Delta S_{Abs}$ $\Delta S_{Des}$	-96 [J/mol K] 112 [J/mol K]	[14]	- 107 [J/mol/K] 110 [J/mol/K]	[18]
$A_{Abs}$ $A_{Des}$	109.4 [1/s] 14.96 [1/s]	[15]	107 [1/s] 520 [1/s]	[19]
$E_{A,Abs}$ $E_{A,Des}$	19.5 [kJ/mol] 15 [kJ/mol]	[15]	14 [kJ/mol] 20 [kJ/mol]	[19]
$d_p$	23 [ $\mu$ m]	[15]	15 [ $\mu$ m]	[15]
$k_s$	1 [W/(m K)]	[16]	1 [W/(m K)]	[16]
$C_p$	500 [J/(kg K)]	[17]	500 [J/(kg K)]	[17]

In the following subsections, modeling details of the MH storage and compressor vessels are provided, i.e., geometries and operative conditions.

### 1) MH-storage vessel

In FIGURE 3, an example of the simulated geometry of the MH-storage vessel including 16 fins for improved heat transfer, and a description of the components can be seen. The modeling was carried out in a 2D geometry to change the number of fins and to analyze the effect on the temperature inside the hydride bed and therefore the hydrogen release. All simulations were run with an automatically generated mesh with adequate quality. During the work, different numbers of fins (0, 4, 8, 12, 16) and the heat distribution inside the storage vessel were considered.

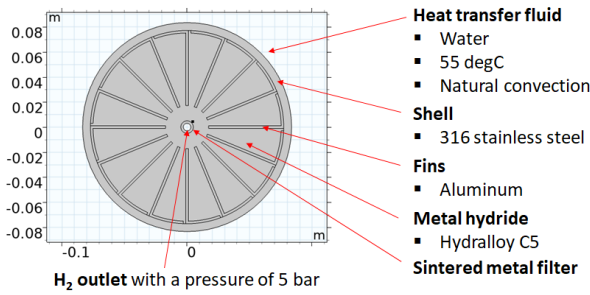


FIGURE 3: GEOMETRY AND COMPONENT DESCRIPTION OF THE MH-STORAGE VESSEL.

For all simulations, the initial temperature was set at 20 °C and natural convection flow on the vessel hull was considered with an external temperature of 55 °C (FIGURE 3). The initial pressure condition in the hydride bed was set at 38 bar of hydrogen and the final pressure at 5 bar of hydrogen (FIGURE 3). Such operative conditions were taken as parameters for coupling the MH vessel with an electrolyzer (initial pressure and temperature conditions) and a fuel cell (final temperature and pressure conditions). As MH-storage material, Hydralloy C5 was used due to its adequate thermodynamic and kinetic behavior for the design of such a MH-storage reservoir. TABLE I shows the most relevant parameters of Hydralloy C5 used for the simulation of the dehydrogenation process.

### 2) MH-compressor vessels

A two-stage MH-compressor was modeled. The key components of an MH-compressor are the pressure vessels and the MH material. In this case, they consist of a cylindrical hull made of stainless steel, which is filled with metal powder and heated and cooled by an external heat transfer fluid (HTF). A sintered filter improves the distribution of hydrogen into the metal bed. Taking into consideration the swelling behavior of the metal hydride bed upon hydrogenation [20], the internal volume of the reservoir was calculated so that the MH material occupied 60-80 % of the internal volume providing free space for the MH material expansion [21]. Each stage consists of a pressure vessel, one for the low-pressure stage and the other for the high-pressure stage. The compressor was modeled in a 2D geometry, and a proper mesh quality was used for the simulations.

The model domain and its most important features are shown in FIGURE 4. The compression cycle was modeled as a batch process.

In the first stage, the following steps took place: inlet of hydrogen into the vessel, exothermic absorption of hydrogen into the metal hydride bed, while the vessel is cooled, closing the inlet and using the sensible heat of the MH-bed to increase the equilibrium pressure of the reaction and endothermically desorbs the hydrogen at a higher-pressure level at this elevated temperature. These steps were repeated in the second stage to further increase the hydrogen pressure.

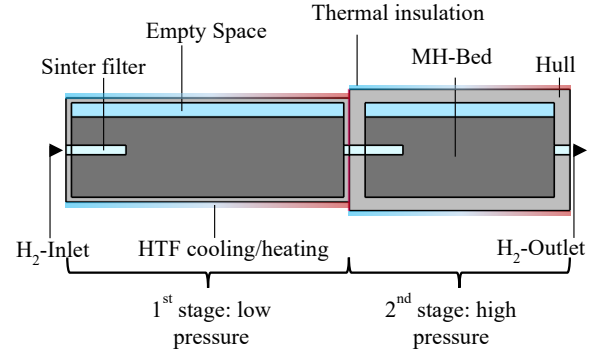


FIGURE 4: GEOMETRY AND COMPONENT DESCRIPTION OF THE MH COMPRESSOR VESSELS.

In this case, Hydralloy C5 was used as the MH-material in the first low-pressure stage and an AB2-material reported previously was employed for the second high-pressure step [18, 19]. The most important properties of these materials can be found in TABLE I.

### D. System simulation

In the following subsection, the main modeling considerations for the system simulation of PEM EL and PEM FC coupled with MH in 0D geometry are provided.

#### 1) EL-MH-storage coupling

The two dynamic 0D models (MH tank and PEM EL) were created using Aspen Custom Modeler® V11 and took into account the equations for mass and energy conservation, chemical reaction kinetics, and thermodynamic properties.

The cell voltage,  $V_{cell}$  [V], of the PEM EL model was calculated according to EQUATION (3):

$$V_{cell} = V_0 + \eta_A + \eta_B - \eta_C + \eta_I \quad (3),$$

where,  $V_0$  is the reversible cell voltage ( $V_{rev}^0$ ) defined by EQUATION (4),  $\eta_A$  and  $\eta_C$  are the anodic and cathodic activation overpotentials accounting for the kinetic, diffusion, and crossover losses,  $\eta_B$  accounts for the overpotential of the electrolyte layer due to the membrane proton conductivity and  $\eta_I$  describes the overpotential caused by interfacial contact and electronic resistances [22].

$$V_{rev}^0 = \Delta G_R^0 / (2 * F) = 1.229 \text{ V} \quad (4),$$

where  $\Delta G_R^0$  is the standard Gibbs free energy of formation of water [kJ/mol] and  $F$  is the Faraday constant, 96485.3 [C/mol].

The model also provides the cell efficiency  $\epsilon_{cell}^{HHV}$  calculated according to the EQUATION 5:



$$\varepsilon_{cell}^{HHV} = \frac{\Delta H_R^0 * \dot{n}_{H_2}}{P_{DC}} = \frac{HHV * \dot{n}_{H_2}}{I_{cell} * V_{cell}} \quad (5),$$

where  $\Delta H_R^0$  [kJ/mol] is the standard formation enthalpy of water,  $P_{DC}$  [W] is the electrical power,  $HHV$  [kJ/mol] is the high heating value of hydrogen,  $\dot{n}_{H_2}$  [mol/h] is the molar flow of hydrogen and  $I_{cell}$  [A] is the electrical cell current.

FIGURE 5 shows a schematic process flowsheet of an EL coupled with a MH tank as well as two secondary flash separators and control devices, likewise valves and an electrical trigger.

The proposed simulation setup allowed the PEM EL to be dynamically controlled when electrical energy is available, e.g., when there is a surplus of wind or photovoltaic power, and to produce hydrogen and oxygen from deionized water by electrochemical water splitting. The water input stream was connected to the anode side, where the oxidation process took place, and thus a mixture of gaseous oxygen and liquid residual water finally left the anode again. Meanwhile, at the cathode side, the electrochemical reduction reaction occurred, in which protons and a certain amount of water that had previously passed through the gas-liquid separation PEM were reduced to molecular hydrogen or released as liquid residual water. The obtained oxygen and hydrogen water mixtures of the anode and cathode, respectively, were separated into gaseous and liquid phases by the two flash separators.

The purified hydrogen was fed into the MH tank, which was cooled during the exothermic absorption process. In turn, the release of hydrogen from the MH tank was an endothermic process and was controlled by the provision of thermal energy via a heat transfer fluid.

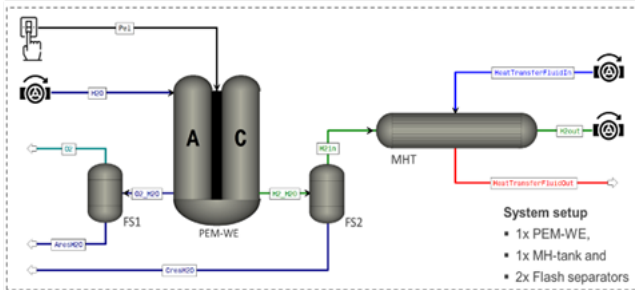


FIGURE 5: FLOWSHEET OF A PEM-EL COUPLED WITH A MH-TANK.

The MH tank simulation was based on the AB<sub>2</sub>-alloy, Hydrallloy C5, described above. The properties of the material employed in the simulations are described in TABLE I. The equilibrium pressure as a function of the temperature of the MH bed was calculated according to the van't Hoff law, as described in EQUATION (1). The intrinsic reaction kinetic was based on EQUATION (2). The thermal properties are based on a lumped effective thermal conductivity of the inner part of the tank and an assumed equidistant spatial distribution.

## 2) FC-MH-storage coupling

A 0D model for the PEM FC was implemented in Matlab/Simulink/Simscape (version R2021a). The model was based on the working principle of a PEM FC governed by redox reactions where hydrogen and oxygen are combined to produce water and heat ( $Q$ ) as a by-product, and electrical power ( $P_{el}$ ) as the main product. In this way, the electrical

power and heat generation are connected. EQUATION 6 describes the whole process:



For the determination of the fuel cell output voltage ( $V_{fc}$ ), the electrical model takes into consideration the thermodynamic output voltage ( $E$ ) minus the activation and ohmic losses ( $R_{ohm} \cdot i_{fc}$ ) from the fuel cell by applying EQUATION 7 [23]:

$$V_{fc} = E - R_{ohm} \cdot i_{fc} \quad (7),$$

The general assumptions of the developed model are: 1. mass transportation losses are neglected, 2. the temperature in the stack is maintained equal to the cathode and anode temperature and 3. humidity levels are kept suitable for any load.

The generated heat can be used for the coupling with the MH-storage tank since the hydrogen desorption is an endothermic reaction, FIGURE 6 shows a conceptual diagram of the PEM FC and MH tank coupling.

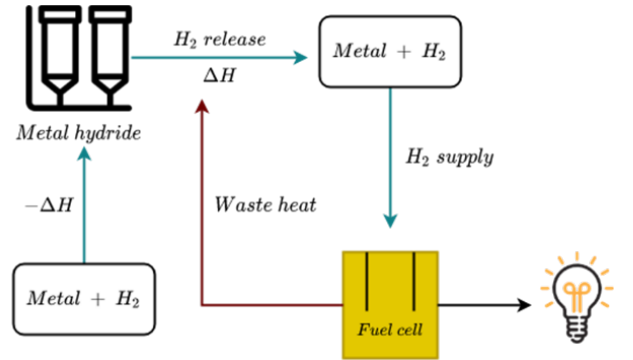


FIGURE 6: DIAGRAM SHOWING A BASIC PEM FC-MH COUPLING CONCEPT.

## III. RESULTS AND DISCUSSION

In this section, the strategies to assemble the SET-Unit are described and developed. In the frame of the development of the project, recent results from ongoing tasks are shown. Furthermore, the prospects and next steps to reach the goals of the project are discussed.

### A. Development and design of metal-hydride (MH) based systems

MH-based systems are the key technology for the development of the SET-Unit concept. The core of the MH systems is the hydride-forming material, M, which interacts with hydrogen by forming the hydride compound as described in EQUATION 8:



As seen, the hydrogen absorption is exothermic and the hydrogen release is endothermic. For the proposed application of MH-storage and compression systems, interstitial hydrides, so-called room temperature hydrides, are the most suitable ones due to volumetric capacity, pressure and temperature range for hydrogen absorption-desorption and ease of

handling. The interstitial hydrides absorb hydrogen by allocating it into the interstitial sites of the crystal structure of the hydride-forming material. Such interstitial hydrides are formed from alloys composed of different metal elements, such as Ti, Cr, Zr, Fe, Al, etc. There is a big variety of hydride-forming alloys which cover a wide range of pressures under mild temperature conditions. For the case of the project, the selected hydride forming alloy can cover operative temperature and pressure range between 20 and 150 °C, and between 1 and 350 bar, respectively, gravimetric capacities between 1 and 3 wt% volumetric capacities ( $> 50 \text{ kg H}_2/\text{m}^3$ ), ease of handling, and scale-up availability [7, 24]. Such room temperature hydrides allow the compact storage of hydrogen in a solid state under mild temperature and pressure conditions and the temperature-driven compression of hydrogen without the need for any mechanical process.

In this section, the development and design of MH-storage and MH-compressor systems for the SET-Unit for efficient solid-state hydrogen storage and compression are discussed.

### 1) Metal-hydride storage

#### 1.1 Hydride forming alloy for large-scale application: characterization and improvement

The metal alloy Hydrallloy C5 is utilized as a solid-state hydrogen storage material for this project because of the suitable thermodynamic stability and hydrogen gravimetric and volumetric capacity. This hydride-forming alloy can absorb hydrogen delivered from an electrolyzer in the range of pressure between 30 and 40 bar at room temperature (around 20 °C). Hydrallloy C5 further has the advantage of uncomplicated handling (stable in ambient conditions), fast activation process, and reasonable kinetic behavior. The operative gravimetric hydrogen capacity of Hydrallloy is between 1.0 and 1.2 wt%, while the volumetric hydrogen capacity is between 50 and 60  $\text{kg H}_2/\text{m}^3$ . FIGURE 7 shows that the maximum capacity of Hydrallloy C5 is reached after 3 hydrogenation-dehydrogenation cycles. During hydrogen cycling, the material undergoes particle size reduction due to the swelling phenomenon. The swelling of the material is caused by the volumetric expansion of the metal lattice at the time to absorb hydrogen and allocate it to the lattice interstices (up to 30 % of volumetric expansion) [21, 25]. The metal alloy used as starting materials presented a size in the mm range ( $\leq 4 \text{ mm}$ ). Due to the swelling phenomenon and considerable stress, the large millimetric particles of the metal alloy split to a size of about 20  $\mu\text{m}$  regardless of the size of the starting material [26]. The MH in such powder form has a low effective thermal conductivity of about  $1 \text{ Wm}^{-1}\text{K}^{-1}$  [17], which leads to low thermal diffusivity upon hydrogenation. This results in the formation of hot spots which slows down the kinetic performance owing to the increase of the equilibrium pressure and subsequent driving force reduction (difference between operative and equilibrium pressure).

The addition of expanded natural graphite (ENG) and pressing the metal alloy into pellets have been already shown to be effective approaches for improving heat conductivity [27]. This approach can be however only scaled up to a certain degree and needs additional experimental effort to find the optimum practical conditions for the formation of the pellets. It was, however, possible to improve the heat conductivity by simply mixing the Hydrallloy C5 with 10wt% of ENG (see FIGURE 7). The peak temperature could be decreased from about 59 °C for pure Hydrallloy C5 to about 56 °C in a

Hydrallloy C5-ENG mixture while retaining most of the hydrogen capacity (1.24 wt% vs. 1.15 wt%).

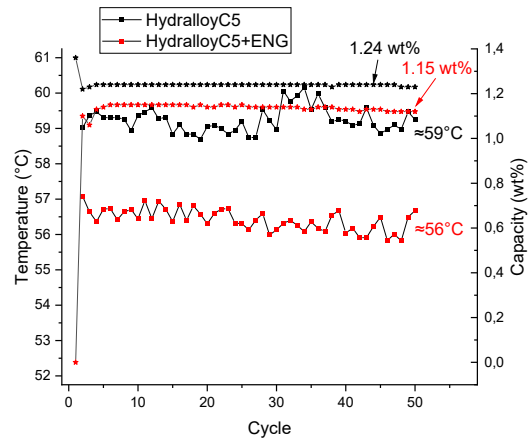


FIGURE 7: COMPARISON OF THE HYDROGEN CAPACITY (STAR-SHAPED DATA POINTS) AND THE MEASURED MAXIMUM TEMPERATURE DURING ABSORPTION (SQUARE-SHAPED DATA POINTS) FOR PURE HYDRALLOY C5 (BLACK) AND WITH A MIXTURE OF HYDRALLOY C5 WITH 10 wt% OF ENG (EXPANDED NATURAL GRAPHITE, RED).

Another challenge of hydrogen storage in metal alloys is stress on the walls of the MH reservoir caused by the swelling upon hydrogenation. Such stress is increased by the decrepitation of the material during cycling, which leads to the compaction of the metal alloy powder at the bottom of the storage vessel. This expansion is in general compensated by leaving free space in the storage vessel, reducing the overall hydrogen gravimetric and volumetric capacity [21]. Experimental results have shown that the addition of ENG and compaction of the Hydrallloy C5 powder can reduce the stress caused by swelling [27]. In other work [28], the effects of the swelling have been reduced by adding small amounts of Aerosil (0.2 wt%), which acts as a gliding agent and especially reduced the friction and compaction of the metal alloy powder at the bottom of the storage vessel [28]. In FIGURE 8, the experimental quantifications of the stress caused by the hydrogenation of Hydrallloy C5 in a full sample holder with a compressed sample and reduced porosity. As seen, the pristine Hydrallloy C5 causes excessive stress after a few cycles. Adding ENG reduces stress, and the combination of ENG and Aerosil further diminish such swelling effects. Mixing ENG and Aerosil with millimetric Hydrallloy C5 material represents a scalable approach for increasing the degree of filling of hydrogen vessels based on MH [29].

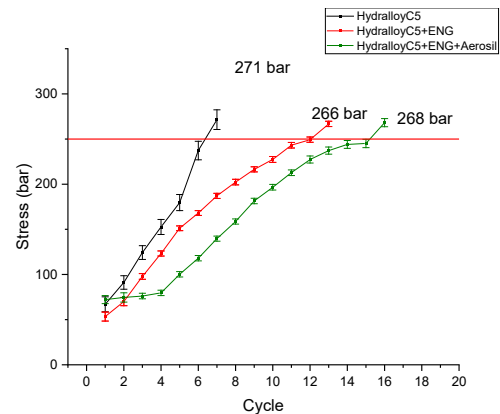


FIGURE 8: COMPARISON OF THE MEASURED STRESS TO THE WALL OF THE REACTION VESSEL DURING CYCLING. FOR THESE EXPERIMENTS, THE METAL ALLOY WAS FURTHER COMPRESSED IN THE SAMPLE HOLDER, TO

REACH THE CRITICAL LIMIT OF <40% POROSITY [21]. THE EXPERIMENTS HAVE BEEN STOPPED, AFTER REACHING THE ELASTIC DEFORMATION LIMIT (250 BAR). IN COMPARISON TO PURE HYDRALOY C5 (BLACK, 6 CYCLES), HYDRALOY C5 + ENG MIXTURE (RED; 13 CYCLES), AND HYDRALOY C5 + ENG + AEROSIL (GREEN; 16 CYCLES).

### 1.2 MH-storage vessel design

The MH-storage system is designed mainly to supply the needed amount of hydrogen for a specific application. To take decisions about the MH-storage reservoir design, a 2D digital model has been developed to investigate the impact of different design parameters applying FEM [30]. The cross-section of the cylindrical MH-storage reservoir with different numbers of fins (0, 4, 8, 12, 16) and for the endothermic dehydrogenation process has been assessed. For the sake of clarity and conciseness, the results obtained from the tank without fins and with 16 fins are here shown. FIGURE 9 shows the temperature distribution inside the storage vessel at different times for the configurations mentioned above.

For the case of the vessel without fins and at 600 seconds (FIGURE 9A), it can be seen that the temperature of the hydride bed close to the wall increases. However, the temperature of the hydride bed at the center of the tank does not appreciably increase. The design with 16 fins (FIGURE 9B) shows that also mostly the shell is heated up, but in this case, the temperature inside the shell is lower than the tank without fins and the fins themselves are heated up slightly. Here, it can also be seen, that only the temperature of the hydride close to the shell or close to the fins is slightly higher than in the center of that tank. This behavior is expected because the fins have far higher thermal conductivity than the metal hydride. The temperature of the shell itself is lower in the fin design because the energy is transferred faster into the center of the vessel by means of fins.

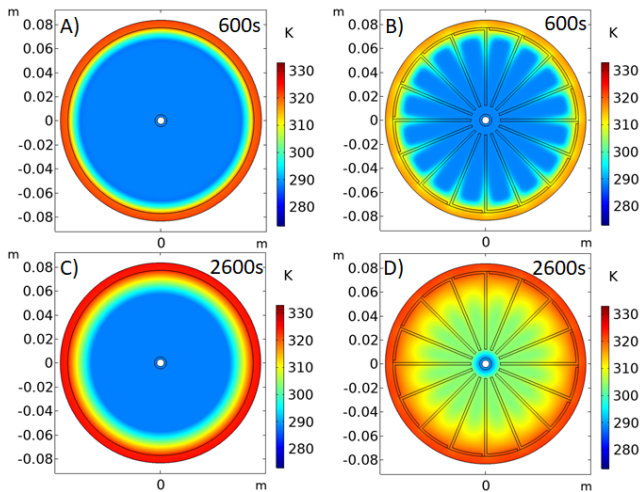


FIGURE 9: TEMPERATURE DISTRIBUTION INSIDE THE TANK VESSEL WITHOUT FINS (A AND C) AND WITH 16 FINS (B AND D) AT 600 s (A AND B) AND 2600 s (C AND D).

After 2600 s, it can be seen that the design without fins is still mostly cold inside the central part of the hydride bed (FIGURE 9C). Only the hydride mass closer to the shell has been heated up. It is also noticed that the temperature drops significantly inside the hydride bed, while the shell is at the same temperature as the heating fluid. This is due to the low effective thermal conductivity of the metal hydride, which results in an ineffective heat diffusivity inside the MH-vessel. On the contrary, in the design with 16 fins after 2600 s (FIGURE 9D), the whole hydride bed is mostly heated. Hence,

the temperature gradient is much lower than the design without fins. Owing to the larger thermal conductivity of the aluminum fins and the effective contact with the MH bed resulting in enhanced effective thermal diffusivity, the internal heat management of the MH-hydrogen vessel is notably improved [31]. These results show that the implementation of fins as a strategy to tackle the poor heat exchange of the MH-bed is a proper approach that leads to a more effective response of the MH-storage vessel at the time to provide hydrogen to a fuel cell device, among other practical applications.

### 1.3 MH-storage system development

The development of the MH-storage system is mainly based on the hydrogen demand from the FC and the coupling with the MH-compressor, as well as the heat exchange management coupling, as depicted in FIGURE 2. As shown in FIGURE 7 and FIGURE 8, the selected room temperature material (Hydralloy C5) presents a capacity of around 1.1-1.2 wt%, swelling issues, and also poor thermal conductivity. The last issue related to internal thermal management of the MH-vessel has been addressed by implementing internal aluminum fins as shown in FIGURE 9. For supplying hydrogen to the planned lab-scale of 10 kWel and the scale-up to a 50 kWel fuel cell, a modular MH-storage system with a total capacity of 10 kg is developed. As seen in FIGURE 10, the system consists of a modular design with 5 MH-storage units containing 4 MH-storage tanks per unit. The whole system can be operated under different dynamic requirements by managing the heat in the units. Schematically, it is proposed to have different numbers of heat exchangers, so that the dynamic response of the system can be coupled with the dynamic of the whole SET-Unit. The hydrogen inlet and outlet lines coming from the electrolyzer and going to the FC or MH-compressors are independently connected by a three-way valve. The connection to the hydrogen lines allows for the charge and discharge of each tank, and even in the configuration with two and four heat exchangers, it is possible to charge and discharge tanks at the same time. The primary heat exchange system provides the cooling source for the hydrogenation process, while the dehydrogenation process is performed by using the waste heat from other devices such as the FC. The proposed configuration makes it possible to connect the MH-storage system with flexibility and to employ the system at different scales.

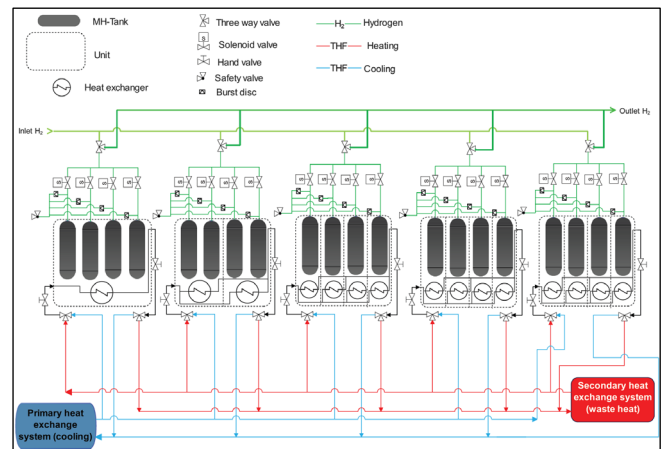


FIGURE 10: FLOW DIAGRAM OF THE MODULAR MH-STORAGE SYSTEM.



## 2) Metal-hydride compressor

### 2.1 Hydride forming alloy for thermally driven compression: development and characterization

In the area of hydrogen compression, metal hydrides have several advantages over the mechanical compressors used nowadays. The absence of moving parts and simple design, coupled with the possible low cost energy source, make metal hydrides a candidate as for hydrogen compressors [32]. Usually,  $AB_2$  type intermetallic are used for high-pressure hydrogen compression, where A stands for Ti/Zr and B stands for mixtures of other transition metals. Hydrogen fills the tetrahedral sites without changing the symmetry of the unit cell. In the frame of Digi-Hydro, a  $TiCr_{1.9}$   $AB_2$  type alloy is investigated as a potential hydrogen compression material for a high-pressure step owing to the simplicity of such binary hydride forming material, high equilibrium pressures, and low cost of its components. However, in some works, it is argued that the hydrogen capacity, as well as the equilibrium pressure, can be increased by adding elements to the alloy, which is not as trivial and reproducible at a larger scale [33]. Determining the enthalpy and entropy values of the synthesized alloy is critical for metal hydride hydrogen compressor design. Obtaining these important parameters serves to determine at what pressure the alloy will absorb or release hydrogen at a given temperature. FIGURE 11A shows the temperature dependence of absorption and desorption plateau pressures of  $TiCr_{1.9}$  alloy. For example, for the  $TiCr_{1.9}$  composition to absorb hydrogen at room temperature,  $H_2$  a pressure above 50 bar at a room temperature of 25 °C is required. The absorbed sample can desorb hydrogen up to a pressure of about 350 bar  $H_2$  when heated to 140 °C. Therefore,  $P_{eq}$ -Temperature curves are very useful because they allow for determining the maximum pressure that the hydrogen compressor can reach under a certain temperature.

When a metal alloy absorbs hydrogen, its unit cell volume expands causing swelling [25]. Determining such volumetric increase is very important for tank design to prevent excessive stress on the internal tank shell. This volume expansion can be calculated by evaluating the diffraction patterns of as-synthesized and hydrogenated material. FIGURE 11B shows the diffraction patterns of the synthesized and hydrogenated samples.

Phase analyses using the Rietveld approach show that the synthesized  $TiCr_{1.9}$  has a C14 Laves phase and a calculated unit cell volume of  $167.5 \text{ \AA}^3$  (cell parameters, a: 4.92 Å, c:7.98 Å). Hydrogenation of the sample causes a shift in the diffraction peaks to lower angles due to the increase in the lattice parameters (FIGURE 11B). The unit cell volume of the hydrogenated phase was calculated as  $193.1 \text{ \AA}^3$  (cell parameters, a: 5.13 Å, c:8.45 Å). This means that there is a 15.3 % increase in the unit cell volume of the sample with hydrogen uptake.

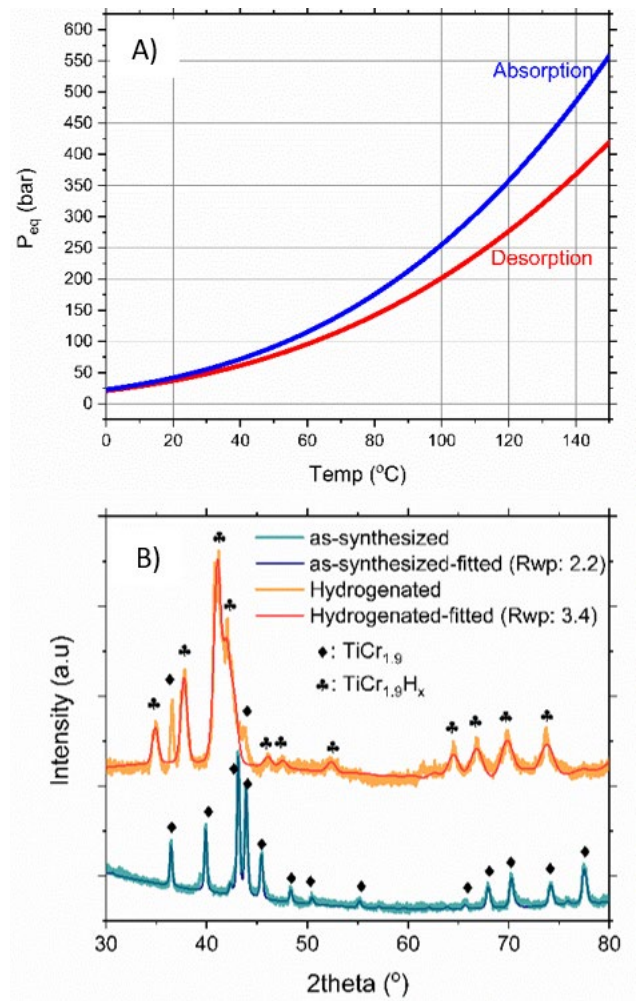


FIGURE 11: A) DEPENDENCE OF ABSORPTION/DESORPTION  $P_{eq}$  ON TEMPERATURE B) DIFFRACTION PATTERNS OF AS-SYNTHESIZED AND HYDROGENATED  $TiCr_{1.9}$ , AS WELL AS FITTED CURVES AFTER RIETVELD REFINEMENT. RWP (%) REPRESENTS THE FITTING GOODNESS.

### 2.2 MH-compressor vessel design

The compression process is a batch process where the pressure vessel and MH-bed are heated up and cooled down repeatedly. Thus, it is necessary to design the vessel considering two important factors. First, an efficient heat transfer to extract the heat released from the exothermal hydrogenation reaction and utilize it for different means. Second, a minimal mass of the pressure vessel shell, so that the energy required for heating up and cooling down is not excessive. Through simulating different configurations of the pressure vessel, a design with improved efficiency for the total compression process can be found.

The shape of the vessel has a strong influence on the heat transfer between the MH-bed, the hull of the vessel, and the external heat transfer fluid, which significantly influences the reaction kinetic behavior of the MH. Especially the diameter D and length L of the cylindrical shell of the compressor vessel and the resulting ratio L/D are important parameters influencing the heat transfer of the compressor. To ensure safety and take into account additional important engineering aspects like cost and manufacturability, during the design, the wall thickness is calculated by Barlow's formula as a function of the diameter [34]

Different diameters and lengths of vessels are investigated. The main challenge in simulating the MH-compressor lies in



modeling the different transient compression steps and the physical coupling between the two stages since two reactions, the desorption of hydrogen in the first stage, and the absorption into the second stage take place simultaneously.

Some preliminary results for the pressure during a complete compression cycle for an unoptimized compressor can be seen in FIGURE 12. This unoptimized compressor configuration has an inner diameter of 4 mm and is filled with 5 kg of Hydroalloy C5 and 4 kg of AB<sub>2</sub> material. The target pressure of 200 bar can be reached at a temperature of 100 °C. The time for the complete compression process is around 16 h, which represents a very long time and is a matter of further optimization.

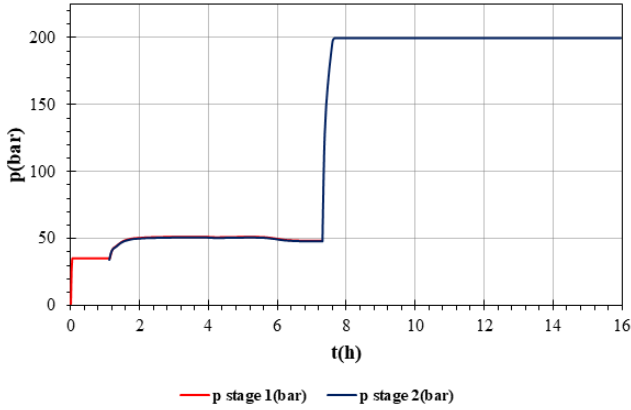


FIGURE 12: PRESSURE DURING COMPLETE COMPRESSION CYCLE IN FEM-SIMULATION OF MH-COMPRESSOR AT AN HTF TEMPERATURE OF 100 °C.

One of the first approaches to improve the performance of the MH-compressor is the improvement of the internal heat management as exposed in FIGURE 9 for the MH- storage system. Moreover, there are also strategies to be implemented for the hydride-forming alloy such as the compaction of the powder [35] or the improvement of the characteristics of the material as described in FIGURE 7 and FIGURE 8.

As part of ongoing work, it is planned to perform the design of a two-stage MH-compressor by employing low and high-pressure hydride forming alloys with more appropriate characteristics such as higher equilibrium pressures at lower temperatures, particularly for the second stage, as shown in FIGURE 11A for the case of TiCr<sub>1.9</sub>, as well as faster kinetic behavior. Two alloys like the ones described in TABLE I will be used. The potential selected alloys were chosen based on the range of temperature and resulting equilibrium pressures and kinetic characteristics. These are Hydralloy C5 and MmNi<sub>5-x</sub>Fe<sub>x</sub> for the low-pressure stage and TiCr<sub>y</sub>-based alloys for the high-pressure stage [21]. Such alloys can be produced in large amounts (~ 30 kg), which represents an intermediate scale for the development of 2-stage MH-compressors. To design the pressure vessel, FEM elements simulations are a powerful tool to predict and improve the hydrogen compression performance of a proposed design.

### 2.3 MH-compressor system development

The metal hydride compressor serves the general purpose to raise the pressure level of hydrogen from the SET-Unit to connect to vehicles equipped with compressed gaseous hydrogen storage. The performance requirements of such compressors are focused on two main premises. On the one hand, the integration of a 2-stage MH-compressor into the SET-Unit defines the compressor size, hydrogen throughput,

and achievable pressure, as well as operating modes, mainly by the availability of hydrogen and energy in the system. On the other hand, the compressor design aims to fulfill the refueling process in terms of pressure level, amount of hydrogen, and refueling frequency.

The compressor will comprise two stages with an AB<sub>5</sub> or AB<sub>2</sub> material (MmNi<sub>5-x</sub>Fe<sub>x</sub> or Hydralloy C5) in the first stage to increase the pressure from the metal hydride storage or directly from the electrolyzer to an intermediate level which is then further increased by an AB<sub>2</sub> material (TiCr<sub>y</sub>-based) in the second stage. The final pressure level is aimed to be suitable for the refueling of storage systems at the 350 bar pressure level, which is the common technology for buses and heavy-duty trucks at the time [36, 37]. However, the achievable pressure level will depend on the characteristics of the material still to be delivered. The general design decision was mainly based on the commercial availability of the hydride forming alloys, the expected temperature levels in the SET-Unit, and the reduced complexity as well as efficiency benefits of a two-stage design compared to three or more stages.

FIGURE 13 shows the working principle of a two-stage metal hydride compressor in the batch process. Each stage comprises a cylindrical vessel containing the hydride forming material and a cooling/heating jacket guiding the heat transfer fluid around it. The setup allows to periodically cool and heat the material and therefore drive the absorption and desorption at a higher pressure, respectively.

The cylinder and heat jacket are one of the proposed potential designs to handle the mass and heat transfer in the compressor. To drive forward the compressor system design, the current work comprises a review of the vessel designs proposed in the literature [21, 38, 39] and transferring them into simple steady-state models. From the heat and mass balances in these models, the amounts of material and energy are derived in the scale that fits the size of the other components of the SET-Unit.

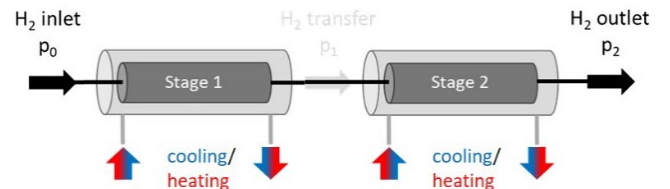


FIGURE 13: FUNCTIONAL PRINCIPLE OF A TWO-STAGE METAL HYDRIDE COMPRESSOR.

As seen in FIGURE 14, the two-stage compressor in continuous operation can be described in a flow diagram showing the main components: the vessels with heat exchangers, piping, and valves. In FIGURE 14, the upper half of the diagram forms one unit, and the lower half forms the second. Both units are alternately cooled or heated by a heat transfer fluid (HTF). Unit 1 is cooled by opening the HTF inlet valve V1.4 and drain valve V1.6. The hydrogen flow is guided by opening V1.1 and closing V1.2 to drive the absorption process in stage 1. Also, stage 2 is absorbing hydrogen coming from the first stage of the second unit. This is possible because unit 2 is heated and thus desorbs hydrogen. After that, the heating/cooling of the two units is inverted and the hydrogen flow is guided by valves V1.1-3 and V2.1-3 accordingly.

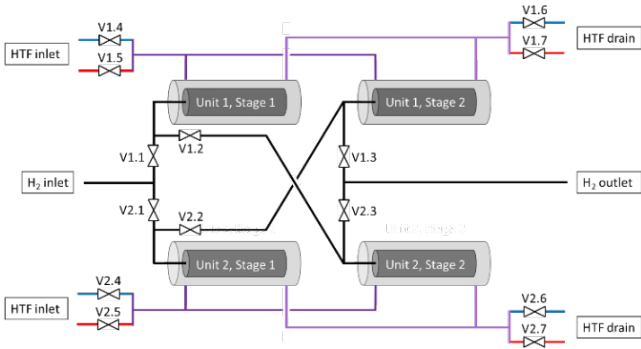


FIGURE 14: FLOW DIAGRAM OF A POTENTIAL TWO-STAGE COMPRESSOR DESIGN FOR CONTINUOUS OPERATION.

Furthermore, the requirements for the coupling with the mobility sector are a matter of ongoing analysis by reviewing updated literature and roadmaps for future hydrogen refueling of long-haul trucks. Published works such as [36, 37, 40, 41, 42] are part of the analysis and represent the technology state of the art. Performance indicators have been identified and compared to the SET-Unit in the intermediate scale (50 kWel). Among the indicators used for comparison, the average flow rate of hydrogen during a filling event stood out as the most challenging for the metal hydride compressor as high amounts of metal hydride material and heating/cooling power would be required. Therefore, different MH-compressor designs and their combination with buffer pressure tanks, allowing for a more time-independent and continuous operation, feasibility, and manufacturability are part of the ongoing analysis to find the optimum design.

### B. Membrane Technology for Hydrogen Processing

A techno-economically viable separation process to extract hydrogen from NG blends underpins the overall feasibility of a trilateral connection between the power, gas, and mobility sectors. Due to its diverse end consumers, hydrogen should be purified to different levels of quality. In comparison to the stationary applications, the requirements specified in the ISO 14687-2 standards for vehicles' PEM fuel cells are significantly more stringent and challenging due to the very low limits of contamination to be achieved. Therefore, our focus is on modeling a separation process customized for the latter applications. A so-called hybrid process taking advantage of both membrane and pressure swing adsorption (PSA) techniques are considered the most promising configuration. In this process scheme, the bulk separation of hydrogen is accomplished in the membrane unit while the following PSA module enhances the final product quality. The process flowsheet as depicted in FIGURE 15 has been developed using Aspen Custom Modeler V12 (ACM) and Aspen Adsorption V12. An envelope-type Matrimid membrane module, which is modeled in ACM, was combined with a 4-bed PSA system. Depending on the downstream applications, the PSA separation can be equipped with two or three layers of adsorbents. The conservation equations of mass, momentum, and energy are simultaneously solved using the finite difference method combined with numerical integration.

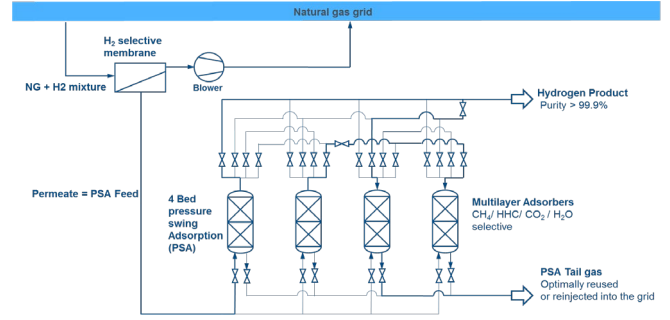


FIGURE 15: A HYBRID SEPARATION PROCESS FOR HYDROGEN RECOVERY AND PURIFICATION.

### C. System Integration

Process and system simulations with the combination of system control and regulation strategies are essential tools for the analysis of sub-systems (bottom-up analysis) and the whole Set-Box (top-down analysis). These tools are also applied for cost-efficient designs and scale-up validations, especially for new conversion and storage energy systems. Different from the 2D or 3D simulations performed applying finite element modeling, 0D models are generally not focused on a single device but are used to model entire systems with multiple interconnected devices [43]. By incorporating the collected information from the spatial finite element simulations and experimentally determined material data, accurate and computationally powerful 0D models can be created. In this section, the first approaches of 0D models for the PEM EL-MH tank and PEM FC-MH tank subsystems and the control for the whole SET-Unit are discussed.

#### 1) PEM EL-MH system

FIGURE 16 illustrates the polarization curve of the PEM EL model including the activation, concentration, and ohmic overpotentials as well as the cell efficiency calculated according to Equation (5).

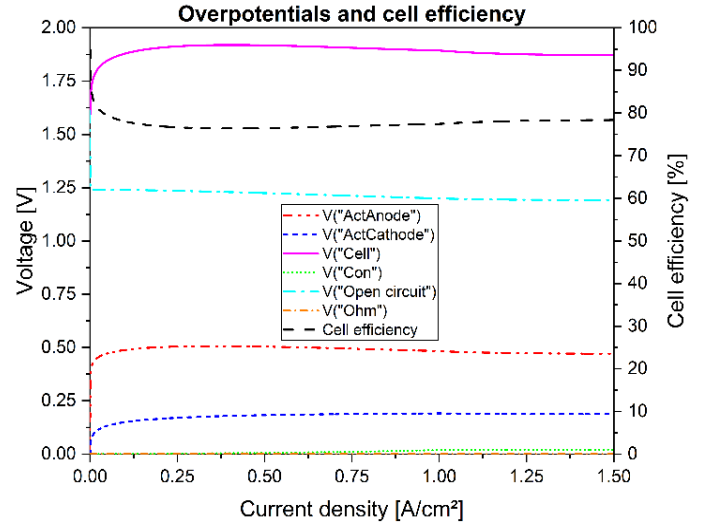


FIGURE 16: SIMULATED OVERPOTENTIALS AND CELL EFFICIENCY

Since the EL operating temperature and pressure have a major impact on the occurring cell voltage, investigations on the optimal process parameters e.g., by the usage of a dynamic digital twin are of great importance. A cold start was simulated at an ambient temperature of 20 °C, which then increased to the final operating temperature of 80 °C and a current density of 1.5 A/cm². The applied electrical power was ramped at 1 kWel/min, which is one of the system boundary conditions

to meet the requirements for a fast system response time. The PEM EL was modeled with a nominal electrical power of 10 kWel with a hydrogen output pressure of 38 bar and, since a hydrogen mass flow of 170 g/h was defined, operated with 8.5 kWel. It is noticeable that the cell voltage drops slightly or rather the cell efficiency increases, although the current density is increased. The reason for this phenomenon is, on the one hand, the temperature increases due to the waste heat generated in the EL and, on the other hand, the pressure and temperature dependence of the electrocatalytic water splitting. According to Arrhenius reaction kinetics, in general, the higher the operating temperature, the better the electrode kinetics and the lower the thermodynamic energy requirement. However, since the membrane must be fully hydrated to avoid degradation problems, the practical usable operating temperature of Nafion-based PEM EL is limited to the boiling point of water or rather the dehydration of the membrane [22].

The concept of a MH tank as a solid-state hydrogen storage system and its design and boundary conditions were previously described: TABLE I and FIGURE 3. This 0D MH tank model simulated a capacity of 695 g of absorbed hydrogen by using about 62.5 kg of room temperature AB<sub>2</sub>-alloy, Hydralloy C5. The mass balances of the AB<sub>2</sub>-alloy, MH, and absorbed hydrogen of the simulated absorption are presented in FIGURE 17.

The absorption process lasted about 250 min with the hydrogen mass flow rate of 170 g/h and a pressure of 38 bar provided by the PEM EL. Assuming a convective heat coefficient of 500 W/(m<sup>2</sup>\*K) for the outer tank shell and a coolant flow of 10 NL/min with a temperature of 20 °C, the tank reached a final temperature of about 25.5 °C. In contrast, the desorption process was simulated at a hydrogen output mass flow of 670 g/h and a defined minimum pressure of 5 bar with a duration of about 60 min. The flow rate of the heat transfer fluid was increased to 60 L/min and applied at a higher temperature of 60 °C. A tank minimum temperature of 15 °C was obtained during the desorption.

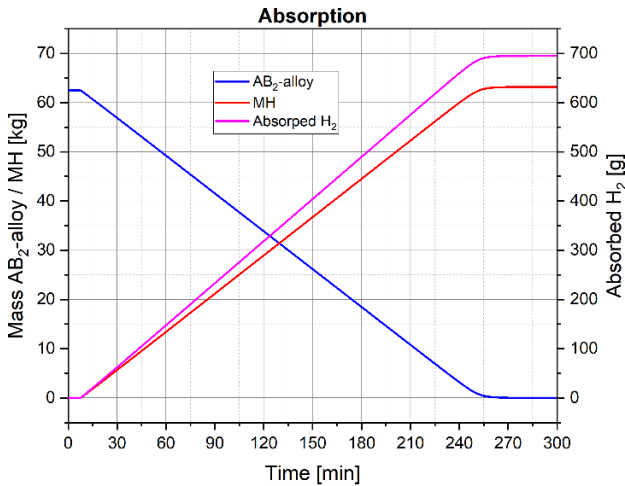


FIGURE 17: MASSES VS. TIME DURING THE ABSORPTION PROCESS [44].

## 2) PEM FC-MH system

A FC is an electrochemical device that converts chemical energy into electrical energy, as described above. Among the different types of fuel cells, PEM FC is the most common one due to its simplicity [45]. PEM FCs are now used mainly for different applications due to their high-power density; low

operating temperature and quick start due to their operation to near ambient temperature [5].

For our laboratory scale, a water-cooled PEM FC stack with a rated power of 5 kWel from the company Power Cellusion is going to be installed [46]. The stack is included in a so-called V5 system additionally having power, fuel, and oxidant control and regulation. The integrated cooling subsystem manages the cooling fluid and produces heat that can be used in our heat management system for coupling it with our metal hydride storage system.

One way of characterizing a FC and analyzing its performance is by obtaining the polarization curve. The polarization curve shows the electrical behavior of the fuel cell and is plotted using the voltage output of the fuel cell in a specific current demand range. According to the electrical losses of the fuel cell, three regions can be described: the activation region, the ohmic region, and the mass transport region. It is desired that the fuel cell be operated in the ohmic region since it is here where it is the most stable. In the activation region, the redox reactions are not happening fast enough and in the mass transport region, the power demand is faster than the reaction rate. FIGURE 18 shows a good agreement with a correlation factor of 0.9 between the modeled and the experimental device polarization for one cell. The simulated curve is based on the electrochemical model described by EQUATION (6) and EQUATION (7) [23]. Both polarization curves are not taking into consideration the mass transport region. The operational range can be defined as a current between 22 A and 105 A where the rated power is reached.

For the efficient coupling of the fuel cell with the MH-storage tank, the model has been improved to first account for the hydrogen flow and thermal interaction between MH-Tank and PEM FC in a steady state. It is also part of the ongoing work modeling the dynamic state under different power demand scenarios to analyze the performance and limits of the PEM FC-MH system. The heat produced by the FC and the temperature in such dynamic power demand scenarios can be calculated by employing the thermal model implemented in Matlab to obtain insights into the regulation and control of heat management.

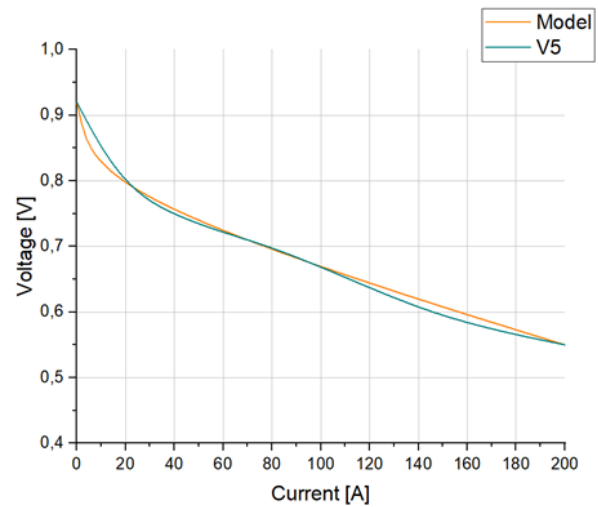


FIGURE 18: COMPARIZATION BETWEEN THE POLARIZATION CURVE FOR THE V5 SYSTEM OF POWER CELLUTION AND THE MATLAB ELECTRICAL MODEL WITH FITTING GOODNESS OF 0.9.



### 3) Control and regulation approaches

The SET-Unit involves the coupling of several devices and systems such as MH-storage, compressor tanks, FC, EL, and membrane gas separation, as shown in FIGURE 1. Each device presents its dynamic response, and therefore a proper control and regulation strategy is necessary to design an efficient coupled system. One of the most important parameters to consider at the time to develop the control and regulation approach for the SET-Unit is the adequate management of the heat. Hydrogen flow and thus the efficiency of the whole system highly depends on heat exchange management. The efficient utilization of the waste heat for hydrogen release as well as cooling demand for charging the MH tanks have to be considered to reduce extensive efficiency losses by including additional energy supply.

As an example of heat coupling and management, in the TecBia project waste heat from a PEM FC was utilized to release hydrogen from 48 MH-tanks [47]. TecBia was built for a maritime onboard power generation of 140 kW. To avoid heat peaks in the FC while switching power levels, seawater in the range of temperatures between 15 and 25 °C was used and the control strategy was carefully analyzed. Another example, but related to stationary applications, is the case of a project using exhaust heat recovery in Japan [48]. The system was designed with the economical objective to generate and store hydrogen during the night and reverse the process during day time since the electricity is cheaper by 50 % at night. Such a system can store 100 Nm<sup>3</sup> of hydrogen. The mechanism of the exhaust heat recovery is not reported and represents one of the key factors for the efficiency of the system.

The projects mentioned above can run in batch mode, which is per se quite challenging. A step forward is the design of such integrated systems to operate in continuous mode. For such purpose, the different components could be controlled independently enabling the possibility to switch between batch and continuous working mode. An operative continuous mode would involve a highly dynamic behavior of the whole system.

FIGURE 19 shows the energy flows to be controlled for the SET-Unit operation. Several components can act either as a heat energy source or sink depending on the configuration and operation mode of the system. Assuming the direct MH-storage and the FC connection, the combination of heat supply from FC and the demand for desorption is sufficient to ensure hydrogen flow to generate electrical power. Considering a third unit, such as MH-compressor requires energy for hydrogen release at the same time, such energy demand can be compensated by a surplus of heat delivered during the absorption of hydrogen in the MH-storage tank connected to the EL.

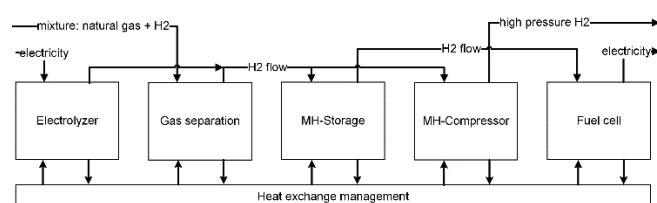


FIGURE 19: SET-Unit SCHEME ENERGY FLOW TO BE CONTROLLED.

To avoid a lack of energy, the operating conditions of the whole system can either be fixed to batch mode, limited to the dynamic operation, or an intermediate mode operation can be implemented. To enable a flexible utilization of the system, a novel complex control strategy must be developed taking into

consideration the critical parameters and the operation modes of the whole system.

## IV. SUMMARY AND PROSPECTS

The Digi-HyPro project aims to develop a modular system, called Smart-Energy-Transform-Box (SET-Unit) to supply decentralized clean energy demands. The SET-Unit serves to optimize the connections between renewable sources and the current power and gas grid demand. This multidisciplinary project involves the engineering of a complex coupled system and the generation of digital twins at different levels, i.e., component (EL, FC, MH-based devices, and gas separation process), subsystem (EL-MH-based devices, FC-MH-storage, etc.), and whole system (SET-Unit) level. Experimental setups of the SET-Unit are developed at the kW range scale. Bottom-up and top-down approaches are applied to design the SET-Unit system.

As part of the bottom-up approach, for the case of the 10 kWel scale, commercial EL and FC devices have been procured and their responses have been characterized based on SIM 0D model simulations. Furthermore, the coupling with the MH-storage system has been tested. Room temperature hydrides have been selected as the core materials for MH-storage and MH-compressor systems because of their adequate storage properties and suitable temperature and pressure conditions for coupling with the FC and EL. A modular MH-storage system with a capacity of 10 kg stored in an AB2 alloy is under development, and its design is based on FEM and the characterization and improvement of the hydride-forming alloy material. Aiming to connect the set box with the mobility sector, a two-stage MH-compression is designed based on FEM and system analyses. The selected materials for the low- and high-pressure stages are AB5 and AB2 room temperature hydrides, respectively. The top-down approach is also part of the investigations and has as aim to investigate and optimize control and regulation strategies for the SET-Unit.

The combination of simulations, experimental setup developments, and the analysis of the whole SET-Unit will allow obtaining information about the responses of the system and its range of applications.

## ACKNOWLEDGMENTS

Funding by dtcc.bw – Digitalization and Technology Research Center of the Bundeswehr – is gratefully acknowledged [project: Digi-HyPro].

## REFERENCES

- [1] Y. Sugiawan, S. Managi, New evidence of energy-growth nexus from inclusive wealth, *Renewable and Sustainable Energy Reviews*, Volume 103, 2019, Pg. 40-48, <https://doi.org/10.1016/j.rser.2018.12.044>
- [2] Our World In Data, <https://ourworldindata.org/fossil-fuels#global-fossil-fuel-consumption> (accessed September 05, 2022).
- [3] NASA Earth observatory, <https://earthobservatory.nasa.gov/features/GlobalWarming/page2.php> (accessed September 05, 2022).
- [4] I.E. Agency, Global Energy Review 2021 - Assessing the effects of economic recoveries on global energy demand and CO2 emissions in 2021, Global Energy, (2021), <https://iea.blob.core.windows.net/assets/d0031107-401d-4a2f-a48b-9eed19457335/GlobalEnergyReview2021.pdf> (accessed September 05, 2022).
- [5] T. Egeland-Eriksen, A. Hajizadeh, S. Sartori, Hydrogen-based systems for integration of renewable energy in power systems: Achievements and perspectives, *Int. J. Hydrogen Energy*, 46 (2021) 31963–31983, <https://doi.org/10.1016/j.ijhydene.2021.06.218>



- [6] I.A. Hassan, H.S. Ramadan, M.A. Saleh, D. Hissel, Hydrogen storage technologies for stationary and mobile applications: Review, analysis, and perspectives, *Renew. Sustain. Energy Rev.* 149 (2021) 111311. <https://doi.org/10.1016/J.RSER.2021.111311>.
- [7] J. Bellosta von Colbe, J.R. Ares, J. Barale, M. Baricco, C. Buckley, G. Capurso, N. Gallandat, D.M. Grant, M.N. Guzik, I. Jacob, E.H. Jensen, T. Jensen, J. Jepsen, T. Klassen, M. V. Lototsky, K. Manickam, A. Montone, J. Puszkiel, S. Sartori, D.A. Sheppard, A. Stuart, G. Walker, C.J. Webb, H. Yang, V. Yartys, A. Züttel, M. Dornheim, Application of hydrides in hydrogen storage and compression: Achievements, outlook and perspectives, *Int. J. Hydrogen Energy*. 44 (2019) 7780–7808. <https://doi.org/10.1016/j.ijhydene.2019.01.104>
- [8] W. Lemberger, M. Groß, M. Miltner, M. Harase, Experimental analysis of membrane and pressure swing adsorption (PSA) for the hydrogen separation from natural gas, *Journal of Cleaner Production* (2017). <https://doi.org/10.1016/j.jclepro.2017.08.012>
- [9] Supporting decarbonization by pipelining H<sub>2</sub> to the point of use [https://www.linde-engineering.com/en/images/H2Tech-Article-Q4-issue-2021\\_tcm19-647879.pdf](https://www.linde-engineering.com/en/images/H2Tech-Article-Q4-issue-2021_tcm19-647879.pdf)
- [10] H. M. Rietveld, A profile refinement method for nuclear and magnetic structures, *J. Appl. Crystallogr.*, vol. 2, pp. 65–71, 1968. <https://doi.org/10.1107/S0021889869006558>
- [11] L. Lutterotti, Total pattern fitting for the combined size-strain-stress-texture determination in thin film diffraction, *Nucl. Instruments Methods Phys. Res. Sect. B Beam Interact. with Mater. Atoms*, 268 (2010) 334–340. <https://doi.org/10.1016/j.nimb.2009.09.053>
- [12] R. Schulz, S. Boily, and J. Huot, Equipment for gas titration and cycling of an adsorbent material E, *CA* 2207149, 1997.
- [13] J.A. Puszkiel, Tailoring the Kinetic Behavior of Hydride Forming Materials for Hydrogen Storage, *Intech. i* (2016) 13. <https://www.intechopen.com/chapters/64686>
- [14] Capurso, G., Schiavo, B., Jepsen, J. et al. Development of a modular room-temperature hydride storage system for vehicular applications. *Appl. Phys.* A 122 (2016) 236. <https://link.springer.com/article/10.1007/s00339-016-9771-x>
- [15] P. S. Krause, J. Warfsmann, E. Wienken, J. Jepsen, T. Klassen, J. Puszkiel, Book of abstract, DIGITAL DEVELOPMENT OF AN OPTIMIZED HEAT MANAGEMENT DESIGN FOR AN INTEGRATED SOLID-STATE H<sub>2</sub>-STORAGE RESERVOIR, page 85” Available: [https://drive.google.com/file/d/10X1tZrIAAmJK7Aoj58QuycTV\\_Qbw8LR/view](https://drive.google.com/file/d/10X1tZrIAAmJK7Aoj58QuycTV_Qbw8LR/view) [last visti 01.9.22]
- [16] V.M. Skripnyuk, M. Ron, Evaluation of kinetics by utilizing the normalized pressure dependence method for the alloy Ti<sub>0.95</sub>Zr<sub>0.05</sub>Mn<sub>1.48</sub>V<sub>0.43</sub>Fe<sub>0.08</sub>Al<sub>0.01</sub>, *J. Alloys Compd* 293 –295 (1999) 385 –390
- [17] S. Suda, Y. Komazaki, N. Kobayashi, Effective thermal conductivity of metal hydride beds. *Journal of the Less Common Metals* 1983, 89 (2), 317–324. DOI: 10.1016/0022-5088(83)90340-5.
- [18] J. Puszkiel, J.M. Bellosta von Colbe, J. Jepsen, S.V. Mitrokhin, E., Movlaev, V. Verbetsky, T. Klassen, Designing an AB<sub>2</sub>-type alloy (TiZr-CrMnMO) for the hybrid hydrogen storage concept. *Energies*, 13(11), 2751, 2020. <https://doi.org/10.3390/en13112751>
- [19] J.A. Puszkiel, J. Bellosta von Colbe, J. Jepsen, V.N. Verbetsky, S.V. Mitrokhin, E.A. Movlaev, T. Klassen, M. Dornheim, Design of an optimized hybrid hydrogen storage reservoir with high capacity. MH2018. Guangzhou, China, 2018.
- [20] O. Gillia, Hydride breathing and its consequence on stresses applied to containers: a review. *Int. J. of Hydrogen Energy*, 46(72) (2021) 35594–35640. <https://doi.org/10.1016/j.ijhydene.2021.07.082>
- [21] M.V. Lototsky, V.A. Yartys, B. Pollet, R.C. Bowman: Metal hydride hydrogen compressors: a review. *International journal of hydrogen energy*, 39(11) (2014) 5818–5851. <https://doi.org/10.1016/j.ijhydene.2014.01.158>
- [22] D. Bessarabov et al., PEM Electrolysis for Hydrogen Production, Florida: CRC Press, 2017. <https://doi.org/10.1201/b19096>
- [23] N.M. Souleman, O. Tremblay, L.A. Dessaint, A generic fuel cell model for the simulation of fuel cell power systems. 2009 IEEE Power and Energy Society General Meeting, PES '09, 1722–1729. <https://doi.org/10.1109/PES.2009.5275853>
- [24] A. Lys, J.O. Fadonougbo, M. Faisal, J.Y. Suh, Y.S. Lee, J.H. Shim, Y. Cho, Y. W. Enhancing the hydrogen storage properties of A<sub>x</sub>B<sub>y</sub> intermetallic compounds by partial substitution: a short review. *Hydrogen*, 1(1)(2020) 38–63. <https://doi.org/10.3390/hydrogen1010004>
- [25] B. Charlas, O. Gillia, P. Doremus, D. Imbault, D. Experimental investigation of the swelling/shrinkage of a hydride bed in a cell during hydrogen absorption/desorption cycles. *Int. J. of Hydrogen Energy* 37 (21) (2021) 16031–16041. <https://doi.org/10.1016/j.ijhydene.2012.07.091>
- [26] F. Qin, L.H. Guo, J.P. Chen, Y.J. Chen, Pulverization, expansion of La<sub>0.6</sub>Y<sub>0.4</sub>Ni<sub>4.8</sub>Mn<sub>0.2</sub> during hydrogen absorption–desorption cycles and their influences in thin-wall reactors. *Int. J. of Hydrogen Energy* 33 (2) (2008) 709–717. <https://doi.org/10.1016/j.ijhydene.2007.10.029>
- [27] C. Pohlmann, L. Röntzsch, F. Heubner, Weißgärber, T.; Kieback, B. Solid-state hydrogen storage in Hydralloy–graphite composites. *J. of Power Sources* 2013, 231 (Suppl. 2), 97–105. <https://doi.org/10.1016/j.jpowsour.2012.12.044>
- [28] D.J. Cuscuna, N. Silin, M. Melnichuk, Stress reduction in a hydride container by the addition of a glidant agent. *Int. J. of Hydrogen Energy* 2020, 45 (51), 27452–27456. DOI: 10.1016/j.ijhydene.2020.07.020.
- [29] J. Warfsmann; M. Passing, P.S. Krause, E. Wienken, J. Jepsen, T. Klassen, J.A. Puszkiel, Easy Up-Scalable Approach to Improve the Properties of Metal-Alloys for Hydrogen Storage, In *23rd World Hydrogen Energy Conference (WHEC 2022)*, Istanbul 26–30 June 2022, Dincer, I., Colphan, C. O., Ezan, M. A., Eds.. ISBN: 978-625-00-0843-0. Available: [https://drive.google.com/file/d/10X1tZrIAAmJK7Aoj58QuycTV\\_Qbw8LR/view](https://drive.google.com/file/d/10X1tZrIAAmJK7Aoj58QuycTV_Qbw8LR/view) [accessed 05.9.22].
- [30] P. S. Krause, J. Warfsmann, E. Wienken, J. Jepsen, T. Klassen, J. Puszkiel, Book of abstract, Digital development of an optimized heat management design for an integrated solid-state H<sub>2</sub>-storage reservoir, In *23rd World Hydrogen Energy Conference (WHEC 2022)*, Istanbul 26–30 June 2022, Dincer, I., Colphan, C. O., Ezan, M. A., Eds.. ISBN: 978-625-00-0843-0. Available: [https://drive.google.com/file/d/10X1tZrIAAmJK7Aoj58QuycTV\\_Qbw8LR/view](https://drive.google.com/file/d/10X1tZrIAAmJK7Aoj58QuycTV_Qbw8LR/view) [accessed 05.9.22].
- [31] A. Mahvash, R. Mane, P. Sharma. Heat transfer techniques in metal hydride hydrogen storage: A review. *Int. J. of Hydrogen Energy* 52 (2017): 30661–30682. <https://doi.org/10.1016/j.ijhydene.2017.10.166>
- [32] M. Lototsky and V. Linkov, Thermally driven hydrogen compression using metal hydrides, *Int. J. Energy Res.* 1–21 (2022). doi: 10.1002/er.8189.
- [33] W. Jiang, C. He, X.-B. Yang, X. Xiao, L. Ouyang, and M. Zhu, Influence of element substitution on structural stability and hydrogen storage performance: A theoretical and experimental study on TiCr<sub>2</sub>-xMnx alloy, *Renew. Energy* 197 (2022) 564–573. doi: 10.1016/j.renene.2022.07.113.
- [34] Verband der TÜV: AD 2000 Regelwerk. 13. Auflage. Berlin: Beuth (Beuth Praxis), 2021.
- [35] J. K. Kim, I. S. Park, K.J. Kim, K. Gawlik, A hydrogen-compression system using porous metal hydride pellets of LaNi<sub>5</sub>-xAlx. *Int. J. of hydrogen energy*, 33(2) (2008) 870–877. <https://doi.org/10.1016/j.ijhydene.2007.10.027>
- [36] H<sub>2</sub> MOBILITY: Wasserstoffbetankung von Schwerlastfahrzeugen – die Optionen im Überblick. H<sub>2</sub> MOBILITY Deutschland GmbH & Co. KG. Berlin, 2021. [Online]. Available: [https://h2-mobility.de/wp-content/uploads/sites/2/2021/10/H2M\\_Ueberblick\\_Betankungsoptione\\_nLNFSNF\\_TankRast\\_2021-10-21.pdf](https://h2-mobility.de/wp-content/uploads/sites/2/2021/10/H2M_Ueberblick_Betankungsoptione_nLNFSNF_TankRast_2021-10-21.pdf). accessed: September 05, 2022
- [37] Y. Rulf, M. Baum, T. Zorn, A. Menzel, A. Rehberger: Fuel Cells Hydrogen Trucks. Heavy-Duty's High-Performance Green Solution. Study Summary. Hg. v. Fuel Cells and Hydrogen Joint Undertaking, Brüssel, 2020. [Online]. Available: <https://www.fch.europa.eu/publications/study-fuel-cells-hydrogen-trucks>. accessed: September 05, 2022
- [38] B.P. Tarasov, B.S. Mikhail, Y.B. Yuri, P.V. Fursikov, M. B. Konstantin M.V. Lototsky, Metal hydride hydrogen compressors for energy storage systems: layout features and results of long-term tests. In: *J. Phys. Energy*, 2020. <https://iopscience.iop.org/article/10.1088/2515-7655/ab6465>
- [39] C. Yehui, Z. Xiangguo, X. Junfeng, K. Huaqin, The comprehensive review for the development of heat exchanger configuration design in metal hydride bed. *Int. J. of Hydrogen Energy* 47 (2022) 2461–2490. <https://doi.org/10.1016/j.ijhydene.2021.10.172>
- [40] R. Peters, J. Breuer, M. Decker, T. Grube, M. Robinius, M. Samsun, C. Remzi, D. Stolten, Future Power Train Solutions for Long-Haul Trucks, *Sustainability* 13(4) (2021) 2225. <https://doi.org/10.3390/su13042225>
- [41] P.K. Rose, F. Neumann, Hydrogen refueling station networks for heavy-duty vehicles in future power systems. P.K. Rose, F. Neumann, Hydrogen refueling station networks for heavy-duty vehicles in future

- power systems. Transportation Research Part D: Transport and Environment D83 (2020) 102358. <https://doi.org/10.1016/j.trd.2020.102358>
- [42] Sinding D., C. Hart, N. Quong, S. Karzel, P. Vyazmina, E. Nouvelot, Q. Ruiz, Requirements for a future refuelling protocol. Deliverable D2.6. Hg. v. Protocol for heavy-duty Hydrogen refuelling (PRHYDE), 2021. [Online]. Available: [https://prhyde-cdn.s3-accelerate.amazonaws.com/wp-content/uploads/2021/07/15080917/PRHYDE\\_Deliverable-D2-6\\_Requirements-for-a-future-refuelling-protocol\\_final.pdf](https://prhyde-cdn.s3-accelerate.amazonaws.com/wp-content/uploads/2021/07/15080917/PRHYDE_Deliverable-D2-6_Requirements-for-a-future-refuelling-protocol_final.pdf). (accessed: September 05, 2022)
- [43] D. M. Dreistadt, J. Puszkiel, J.M. Bellosta von Colbe, G. Capurso, G. Steinebach, S. Meilinger, J. Jepsen, A Novel Emergency Gas-to-Power System Based on an Efficient and Long-Lasting Solid-State Hydride Storage System: Modeling and Experimental Validation, *Energies* 15 (2022) 844. <https://doi.org/10.3390/en15030844>
- [44] E. Wienken, P. Krause, J. Warfsmann, J. Bellosta von Colbe, J. Jepsen, T. Klassen, J. Puszkiel, Book of abstract, Modeling and process simulation of a metal hydride tank coupled with a PEM electrolyzer, In *23rd World Hydrogen Energy Conference (WHEC 2022)*, Istanbul 26-30 June 2022, Dincer, I., Colphan, C. O., Ezan, M. A., Eds.. ISBN: 978-625-00-0843-0. Available: [https://drive.google.com/file/d/10X1tZrIAAmJK7Aoj58QuyctCV\\_Qbw8LR/view](https://drive.google.com/file/d/10X1tZrIAAmJK7Aoj58QuyctCV_Qbw8LR/view) [accessed: September 05, 2022].
- [45] V. Mehta, Cooper, J.S. Review and analysis of PEM fuel cell design and manufacturing. *J. Power Sources* 2003, 114, 32–53.
- [46] Power Cellution, <https://powercellution.com/power-generation-system-5> (accessed: September 05, 2022)
- [47] M. Cavo, E. Gadducci, M. Rivarolo, L. Magistri, A. Dellacasa, M. Romanello, G. Borgogna, C. Davico, Thermal integration of PEM Fuel Cells and metal hydrides storage system for Zero Emission Ultimate Ship (ZEUS), *E3S Web of Conferences* 334, 04004, 2022.
- [48] Ø. Ulleberg, H. Ito, M. H. Maack, B. Ridell, S. Milese, N. Kelly, A. Iacobazzi, Modeling and Evaluation of Hydrogen Demonstration Systems, *WHEC* 16 / 13, 2006.